Interaction between the T4 Helicase-Loading Protein (gp59) and the DNA Polymerase (gp43): A Locking Mechanism to Delay Replication during Replisome Assembly†

Jun Xi,‡ Zhihao Zhuang,‡ Zhiquan Zhang,§ Tzvia Selzer,‡ Michelle M. Spiering,‡ Gordon G. Hammes,§ and Stephen J. Benkovic*,‡

Department of Chemistry, Pennsylvania State University, 104 Chemistry Building, University Park, Pennsylvania 16802, and Department of Biochemistry, Duke University Medical Center, Box 3711, Durham, North Carolina 27710

Received September 22, 2004; Revised Manuscript Received November 1, 2004

ABSTRACT: The T4 helicase-loading protein (gp59) has been proposed to coordinate leading- and lagging-strand DNA synthesis by blocking leading-strand synthesis during the primosome assembly. In this work, we unambiguously demonstrate through a series of biochemical and biophysical experiments, including single-molecule fluorescence microscopy, that the inhibition of leading-strand holoenzyme progression by gp59 is the result of a complex formed between gp59 and leading-strand polymerase (gp43) on DNA that is instrumental in preventing premature replication during the assembly of the T4 replisome. We find that both the polymerization and 3′ → 5′ exonuclease activities of gp43 are totally inhibited within this complex. Chemical cross-linking of the complex followed by tryptic digestion and peptide identification through matrix-assisted laser desorption/ionization−time-of-flight (MALDI-TOF) mass spectrometry identified Cys169 of gp43 and Cys215 of gp59 as residues in a region of a protein−protein contact. With the available crystal structures for both gp43 and gp59, a model of the complex was constructed based on shape complementarity, revealing that parts of the C-terminal domain from gp59 insert into the interface created by the thumb and exonuclease domains of gp43. This insertion effectively locks the polymerase into a conformation where switching between the pol and editing modes is prevented. Thus, continued assembly of the replisome through addition of the primosome components and elements of the lagging-strand holoenzyme can occur without leading-strand DNA replication.

Bacteriophage T4 provides one of the better-developed systems for analyzing in detail the mechanism of DNA replication (*1*−*3*). Whether initiated by either an origin- or recombination-dependent mode, T4 replication requires a phage-induced DNA polymerase (gp43),[1] which forms the holoenzymes with clamp (gp45) and clamp loader (gp44/62) proteins to carry out the continuous synthesis of the leading strand and the discontinuous synthesis of Okazaki fragments on the lagging strand. The gp43 protein possesses a 5′ → 3′ polymerizing activity and a 3′ → 5′ exonuclease (proofreading) activity (*4*) and is positioned on the DNA template by the circular trimeric sliding gp45 clamp, which in turn is loaded by the gp44/62 clamp loader.

For the holoenzyme to advance through a DNA duplex, the hexameric helicase gp41 (*5*), an essential constituent of the T4 primosome, is required to move 5′ → 3′ on the lagging strand and to unwind the double-stranded DNA ahead of the DNA polymerase in an ATP- or GTP-driven process (*6*). The helicase interacts with the primase (gp61), another protein of the T4 primosome, dramatically increasing its rate of synthesis of the RNA primer used to initiate lagging-strand DNA synthesis. Although gp41 helicase can add to forked DNA templates by itself, its loading is much more rapid when the helicase-loading protein (gp59) is present (*7*). The maximum activity of DNA unwinding occurs when gp41 and gp59 are in a 1:1 ratio (*8*), and the maximal priming rate also occurs when gp61 and gp41 are present in a 1:1 molar ratio (*9*). On the lagging strand of the replication fork, the T4 single-stranded binding protein (gp32) coats the single-stranded DNA template strand and also increases the rate of primer synthesis (*10*). In addition, gp32 increases the processivities of both the lagging-strand DNA polymerase

† This research was supported by Grants from the National Institutes of Health, GM65128 (to G.G.H.), GM071130 (to M.M.S.), and GM13306 (to S.J.B.).

* To whom correspondence should be addressed: Pennsylvania State University, 414 Wartik Laboratory, University Park, PA 16802. Telephone: (814) 865-2882. Fax: (814) 865-2973. E-mail: sjb1@psu.edu.

‡ Pennsylvania State University.

§ Duke University Medical Center.

[1] Abbreviations: P−T junction, primer−template junction of duplex DNA; gp32, single-stranded DNA-binding protein; gp41, helicase; gp43, DNA polymerase; gp43(exo-), exonuclease-deficient gp43; gp44/62, clamp loader; gp45, processivity clamp for DNA polymerase; gp59, helicase-loading protein; gp61, primase; OG, Oregon Green 488; CPM, 7-diethylamino-3-(4′-maleimidylphenyl)-4-methylcoumarin; A488, Alexa Fluor 488; A555, Alexa Fluor 555; FRET, fluorescence resonance energy transfer; BMH, 1,6-bismaleimidohexane; BMDB, 1,4-bismaleimidyl-2,3-dihydroxybutane; BSA, bovine serum albumin; Tris, tris(hydroxymethyl)aminomethane; HEPES, 4-(2-hydroxyethyl)-1-piperazineethanesulfonic acid; SDS, sodium dodecyl sulfate; DTT, dithiothreitol; EDTA, ethylenediamine tetraacetic acid, disodium salt; dNTP, deoxynucleotide triphophate; ATP, adenosine triphosphate; GTP, guanosine triphosphate; PAGE, polyacrylamide gel electrophoresis; MALDI−TOF, matrix-assisted laser desorption/ionization−time-of-flight.

10.1021/bi0479508 CCC: $30.25
Published on Web 01/29/2005

and the T4 encoded 5′ → 3′ nuclease (RNaseH) that removes the RNA primers and some adjacent DNA, before adjoining Okazaki fragments are joined by DNA ligase (*11*).

Among the four proteins involved in primosome assembly, the gp59 helicase-loading protein, a small (26 kDa) basic protein that has been shown to bind each of the other three proteins, is critical to how the replisome assembles and functions. Chemical cross-linking studies informed by the crystal structures of gp59 (*12*) and gp32 (*13*) have delineated the specific area of close interaction between gp59 and gp32 (*14*), as well as between gp59 and gp41 (*15*). These cross-linking experiments also prove that gp59 induces the oligomerization of gp41 to form a hexameric-ring structure (*15*). The crystal structure of gp59 reveals a two domain, almost completely helical protein with a shallow central groove between these domains on the top surface of the protein (*12*). The protein has no structural similarity to those of single-stranded DNA-binding proteins and no sequence similarity to those of other helicase-loading proteins, such as DnaC from *Escherichia coli*. However, a portion of the N-terminal domain shares strong structural similarity with several members of the high-mobility group (HMG) family proteins, which similar to gp59, bind branched DNA structures. Gp59 binds both single- and double-stranded DNA, although it has a higher affinity for the forked DNA substrate (*12*, *16*, *17*).

Besides loading helicase on gp32-coated single-stranded DNA, the role of gp59 in T4 replication is still being revealed. The helicase-loading protein is essential for recombination and recombination-dependent replication (*18*, *19*) *in vivo*. *In vitro*, gp59 has been shown to promote DNA synthesis from a preformed R loop within the T4 *uvsY* origin (*20*). It has been proposed that gp59 protein may first bind to the fork at an origin or a recombination intermediate and then attract the helicase and gp32 to the fork arm that will become the lagging-strand template (*21*). In the presence of gp32, UvsX, UvsY, and gp41, gp59 facilitates branch migration (*22*, *23*).

Numerous studies (*24*−*28*) have suggested that the process of replication fork unwinding by the T4 primosome might be functionally coupled to the movement of the holoenzymes through specific protein−protein interactions. Although such contacts have been well-established in similar systems, such as between the helicase/primase protein and the T7 DNA polymerase in the bacteriophage T7 system (*29*) and the DnaB helicase and the τ subunit of the DNA polymerase III holoenzyme in *E. coli*, which increases the unwinding activity of DnaB by 10-fold (*30*). Evidence for physical contacts between the holoenzyme and primosome units in the T4 system stems only from a recent finding of an interaction between gp59 and gp43 polymerase by chemical cross-linking and fluorescence resonance energy transfer (FRET) methods (*31*).

This interaction can rationalize the observed inhibition of the leading-strand holoenyzme progression by gp59 in terms of creating a steric block by gp59 at the replication fork ahead of the polymerase (*21*). Inhibition by gp59 was detected in studies of DNA synthesis from a preformed T4 R loop in the absence of helicase (*20*) and of leading-strand DNA synthesis on a forked template by wild-type T4 polymerase (*21*). It had also been observed that gp59 protein inhibited strand-displacement synthesis from a nicked plasmid in reactions without the helicase (*32*). In all cases, the inhibition was not observed in the presence of both gp41 helicase and gp32. Conceivably, gp59 helps coordinate leading-strand holoenzyme and primosome assembly by blocking leading-strand DNA synthesis when either helicase gp41 or single-stranded binding protein gp32 is missing.

The goal of this work is to demonstrate that the inhibition of leading-strand holoenzyme progression by gp59 is the result of a complex formed between gp59 and gp43 on DNA and to further establish the biological significances of this inhibition in the T4 replication. These studies have revealed that the gp43−gp59 complex is capable of inhibiting both polymerization and exonuclease activities of gp43, which can be rationalized by our protein−protein interaction model between gp43 and gp59, where gp59 effectively locks gp43 into a specific conformation that prevents the partitioning of DNA substrate between the polymerization and exonuclease sites.

MATERIALS AND METHODS

All fluorescent dyes were purchased from Molecular Probes. [γ-^{32}P]ATP and [α-^{32}P]dCTP were purchased from New England Nuclear. Unlabeled deoxynucleotides and ribonucleotides were purchased from Roche Biochemicals. Bacteriophage T4 proteins: exonuclease-deficient gp43 [gp43(exo-)] (*33*), wild-type gp43 (*33*), gp44/62 (*34*), gp45 (*35*), gp32 (*36*), and gp59 (*14*) were purified as previously described. All other chemicals were of analytical grade or better. All of the data from titration experiments were analyzed by KaleidaGraph (Synergy Software) and fit with the following empirical equation:

$$Y = A_1 + \frac{A_2 - A_1}{1 + \dfrac{EC_{50}{}^{n}}{X^n}}$$

where A_1 is the initial response in the absence of gp59, A_2 is the final response in the presence of gp59, Y is the observed response at concentration X, which is the total concentration of gp59 in the mixture, EC_{50} is the concentration of gp59 that produces a response halfway between the baseline and maximum responses, and n is the Hill coefficient.

Forked DNA Substrates. Forked DNA substrates were constructed as previously described (*37*). The large forked DNA substrate (34/62/50-mer) was prepared from a 34-mer primer (5′-ACTCCTTCCGCACGTAATTTTTGACGCAC-GTTGT-3′) annealed to a 62-mer leading-strand template (5′-ACACAGACGTACTATCATGACGCCATCAGACAA-CGTCGTCAAAAATTACGTGCGGAAGGAGT-3′) and a partially complementary 50-mer lagging-strand template (5′-AGGGTGGGTGGGAGGGTGGGTTGGAGGGAGTG-GGATGATAGTACGTCTGTGT-3′). A biotinylated large forked DNA substrate (34/62/bio50-mer) was prepared as above but with a 3′-end biotinylated 50-mer lagging-strand template of the same sequence (Integrated DNA Technologies, Inc.). A similar small forked DNA substrate (34/62/25-mer) was prepared from the same primer and leading-strand template as above and a partially complementary 25-mer lagging-strand template (5′-GAGTGGGAT-GATAGTACGTCTGTGT-3′).

Preparation of gp59 Mutants. The gene encoding the helicase-loading protein was isolated from bacteriophage T4 genomic DNA by polymerase chain reaction (PCR) amplification using the following primers: A, 5′-GCGGAATTC-CTAGATGATTAAACTCCGC-3′, and B, 5′-GGTGGT-TGCTCTTCCGCAATACTTGCAAGATTTCAC-3′. The product was digested with *Bfa*I and *Sap*I and then ligated into a modified IMPACT vector (New England Biolabs) digested with *Nde*I and *Sap*I. This vector places a self-cleaving intein and chitin-binding domain at the C terminus of gp59 under the control of a T7 promoter and allows affinity purification on a chitin column followed by cleavage of the intein with dithiothreitol (DTT) to produce the wild-type gp59 in high yield.

The C42A mutation in gp59 was introduced by primer overlap extension. The expression plasmid IMPACT-gp59 was used as the template. In brief, two independent PCR amplifications were conducted; the first reaction utilized primer A and mutagenic reverse primer C, 5′-CAGACAC-CCGCATCGCCCAATTATAC-3′; the second reaction utilized primer B and mutagenic forward primer D, 5′-GTA-TAATTGGGCGATGCGGGTGTCTG-3′. The resulting products were gel-purified and then used in a subsequent PCR reaction, employing primers A and B.

The C215A mutation in gp59 was introduced by PCR amplification using the expression plasmid IMPACT-gp59 as the template, primer A (described above), and primer E, 5′-GGTGGTTGCTCTTCCGCAATACTTAGCAGATT-TCACAGTTTC-3′. The desired expression construct was obtained by restriction digestion of the final product with *Bfa*I and *Sap*I, followed by ligation into the vector fragment of IMPACT-gp59 cleaved with the *Nde*I and *Sap*I.

Following plasmid amplification in *E. coli* DH5α-E strain, the desired mutations were confirmed by DNA sequencing. Mutant proteins were expressed and purified as described previously (*14*).

Protein Labeling. The protein labeling through cysteine modification was carried out as follows: gp59 or gp59-(C42A) was dialyzed in labeling buffer 20 mM tris(hydroxymethyl)aminomethane (Tris) (pH 7.5), 150 mM NaCl, and 10% glycerol for 8 h and was incubated with a 5-fold excess of 7-diethylamino-3-(4′-maleimidylphenyl)-4-methylcoumarin (CPM) or Alexa Fluor 555 C2 maleimide (A555) for 4 h. The N-terminal labeling of proteins was performed according to the following procedure: gp43(exo-) or gp59 was dialyzed in labeling buffer 25 mM 4-(2-hydroxyethyl)-1-piperazineethanesulfonic acid (HEPES) (pH 6.8), 150 mM NaCl, and 10% glycerol for 8 h at 4 °C and was labeled with a 3-fold excess of Oregon Green 488 carboxylic acid, succinimidyl ester, 5-isomer (OG), Alexa Fluor 488 carboxylic acid, succinimidyl ester (A488), or biotinamidocaproate *N*-hydroxysuccinimide as required (*31*). The labeled proteins in all cases were then dialyzed in labeling buffer at pH 7.5 containing 10 mM β-mercaptoethanol to remove the unlabeled dye and frozen in aliquots at −70 °C. All labeling processes were performed at 4 °C and in less than 30 h to minimize any reduction in wild-type activities. The activities of the labeled proteins were compared to the unlabeled proteins in the full replication assays (*36*), and no significant differences were found.

Functional Assay of gp43 Polymerase Activity on the Forked DNA. The small forked DNA substrate 34/62/25-mer (100 nM) (the primer strand 34-mer had been labeled with ^{32}P phosphate at its 5′ end using T4 polynucleotide kinase) was preincubated with 150 nM gp43(exo-) and 0−1800 nM gp59 in 20 μL polymerization buffer (25 mM HEPES at pH 7.5, 8 mM $Mg(OAc)_2$, 40 mM NaOAc, and 5 mM DTT) at 25 °C for 5 min. After the addition of dNTPs (250 μM final concentration), the reactions were allowed to proceed for 30 s at 25 °C and then quenched with an equal volume of 0.5 mM ethylenediamine tetraacetic acid, disodium salt (EDTA) and a double volume of loading dye with 1.9% sodium dodecyl sulfate (SDS). The mixture was separated by electrophoresis on a 12% denaturing polyacrylamide gel followed by phosphorimaging analysis. The progress of each reaction was determined by quantifying the amount of elongated primer, which was calculated from the difference between the amount of the initial primer and the amount of the remaining primer.

Equilibrium FRET Titration of OG-gp43(exo-) by CPM-gp59(C42A). Equilibrium FRET experiments were performed using an ISA (Edison, NJ) Fluoromax-2 spectrofluorometer. Slit widths were adjusted appropriately between 2 and 4 nm to keep the spectrum on scale. The integration time was 0.5 s. FRET experiments using CPM as a donor were excited at 385 nm, and its emission spectra were recorded between 400 and 600 nm. The acceptor OG sensitization was measured at 520 nm and corrected for background fluorescence because of direct excitation of the acceptor. The distance between the donor and acceptor was calculated as described previously (*38*).

Concentrations ranging from 0 to 1800 nM for CPM-gp59-(C42A), 150 nM for OG-gp43(exo-), and 100 nM for the DNA (62/34/25-mer) were allowed to equilibrate in the polymerization buffer at 25 °C for at least 10 min before the measurements were taken. Control experiments to quantify the emission of the acceptor OG-gp43(exo-) because of direct excitation at the donor excitation wavelength were performed exactly as above except for substitution of CPM-gp59(C42A) by unlabeled gp59(C42A) at identical concentrations. The acceptor-only spectrum was subtracted from the donor−acceptor spectrum to obtain the final result for each measurement at each concentration of gp59.

RsaI Digestion of the Forked DNA. The large forked DNA substrate 34/62/50-mer (100 nM) (both the primer-strand 34-mer and the lagging-strand 50-mer had been labeled with ^{32}P phosphate at their 5′ ends using T4 polynucleotide kinase) was preincubated with 0−1500 nM gp59 and 150 nM gp43(exo-) in 20 μL of polymerization buffer at 25 °C for 5 min. After the addition of *Rsa*I (5 units), the reactions were allowed to proceed for 30 s at 25 °C and were then quenched with an equal volume of 0.5 mM EDTA and a double volume of loading dye containing 1.9% SDS. The mixture was separated on a 12% denaturing polyacrylamide gel followed by phosphorimaging analysis. The progress of each reaction was determined by quantifying the amount of digestion product.

Functional Assay of Wild-Type gp43 3′ → 5′ Exonuclease Activity. The small forked DNA substrate 34/62/25-mer (100 nM) (the primer strand 34-mer was labeled with ^{32}P phosphate at its 5′ end using T4 polynucleotide kinase reaction) was preincubated with 0−1800 nM gp59 in 20 μL of polymerization buffer at 25 °C for 5 min. After the addition of 150 nM of wild-type gp43, the reactions were

allowed to proceed for 30 s at 25 °C and were then quenched with an equal volume of 0.5 mM EDTA and a double volume of loading dye with 1.9% SDS. The mixture was separated on a 12% denaturing polyacrylamide gel followed by phosphorimaging analysis. The progress of each reaction was determined by quantifying the amount of hydrolyzed 34-mer primer.

Single-Molecule FRET. Single molecules were observed with a home-built fluorescence microscope using total internal reflection optics. A Zeiss microscope with a 100×, 1.45 aperture, oil immersion lens and a Pentamax ICCD camera was employed to detect single molecules. The microscope filters were set to observe fluorescence from three different sources: F1, emission from donor A488 (excitation at 488 nm/emission at 510−540 nm); F2, emission from energy transfer between A488 and A555 (excitation at 488 nm/emission at 595−645 nm); and F3, emission from acceptor A555 (excitation at 514 nm/emission at 535−585 nm). Experiments were performed at ambient temperature, ~25 °C. All single-molecule experiments were performed in triplicate, and in all cases, well-resolved fluorescent spots were observed.

The forked DNA (34/62/bio50-mer) was attached to a glass slide prepared with avidin on the surface (*39*) as follows: a solution containing 100 nM forked DNA (34/62/bio50-mer), 15 μM bovine serum albumin (BSA), and 0.1 M Tris (pH 7.0) was passed 3 times through the space between the cover slip and avidin-coated slide. The slide was allowed to incubate for 30 min and then was washed 3 times with Tris buffer (without BSA). The concentration of avidin on the slide was adjusted to observe well-separated fluorescent spots in the microscope field judged to be due to individual forked DNA molecule coated with fluorescently labeled proteins. Previously, the identical conditions for coating the slides with avidin resulted in the presence of single molecules established by catastrophic photobleaching (*39*). Also, 3′-biotin, 5′-fluorescein-labeled single-stranded DNA binds to the slide, and the resultant fluorescent spots photobleached as single molecules.

The first protein to be added in a given experiment was passed through a slide with bound forked DNA substrate 3 times and allowed to stand for 10 min. As required by the experiment, 100 nM fluorophore-labeled or unlabeled protein in Tris buffer was used. The protein not bound to the forked DNA was then washed away with three aliquots of buffer. Subsequent protein or reagent additions were carried out on the microscope stage without moving the slide in three similar applications. This served to wash away the previous unbound protein, and only an excess of the final protein or reagent was left on the slide. Fluorescent spots are observed only in the presence of a biotinylated forked DNA substrate, demonstrating that nonspecific binding of proteins to the slide does not occur.

Functional Assay of gp43 Polymerase Activity on the TFRII M13 DNA Substrate. The tailed replicative form II (TRFII) M13 DNA substrate was synthesized as previously described (*40*). Replication reactions were carried out in a complex buffer containing 25 mM Tris-acetate (pH 7.5), 125 mM KOAc, and 10 mM $Mg(OAc)_2$. The typical reaction (60 μL) contains 2 nM TRFII DNA substrate, 16 nM gp43(exo-), 100 nM gp45 (as the trimer), 18 nM gp44/62, 4 μM gp32, 200 nM gp59, 1 mM ATP, 50 μM each of dATP, dGTP, dCTP, and dTTP, and [α-^{32}P]dCTP [3000 Ci/mmol]. For each reaction, the holoenzyme was allowed to assemble onto the DNA at 37 °C for 30 s, followed by the addition of the remaining primosome proteins, unless the late addition of gp59 was required by the experiments. The mixture was incubated at 37 °C for 2.5 min, and the reaction was initiated with the addition of dNTPs (final concentration). Reaction aliquots were withdrawn at various times, quenched with an equal volume of 0.5 mM EDTA and a double volume of loading dye and separated by electrophoresis on a 0.6% alkaline agarose gel, followed by phosphorimaging analysis.

Mapping the Site of Interaction between gp59 and gp43. All proteins subjected to cross-linking were dialyzed into labeling buffer before the reaction. 1,6-Bismaleimidylhexane (BMH, Pierce) or 1,4-bismaleimidyl-2,3-dihydroxybutane (BMDB, Pierce) was dissolved in *N*,*N*-dimethlyformamide to a concentration of 200 μM. A total of 1 μL of this solution was added to 19 μL of a solution containing 0.5 μM gp43-(exo-) and 1.5 μM gp59 in the absence or presence of 0.25 μM large forked DNA substrate. The reaction was allowed to proceed for 10 min and was quenched with the addition of 5 μL of SDS−PAGE buffer (60 mM Tris at pH 6.8, 2% SDS, 0.1% bromphenol blue, 25% glycerol, and 108 mM β-mercaptoethanol). The samples were separated and analyzed by 6% SDS−PAGE.

The Western blot analyses were done by using a combination of an anti-gp43 antibody and neutravidin horseradish peroxidase conjugate when the N terminal of gp59 was labeled with biotin. The proteins were transferred to a nitrocellulose membrane, and the membrane was blocked for 2 h at room temperature with 3% BSA in 20 mM Tris at pH 7.6, 140 mM NaCl, and 0.1% Tween 20 (TBST). To detect the presence of gp43, the membrane was incubated with a 1:3000 dilution of the anti-gp43 antibody in TBST with 3% BSA for 10 h at 4 °C and was then washed with TBST (4 × 10 min each) followed by incubation with a 1:5000 dilution of anti-rabbit IgG antibody linked to horseradish peroxidase (Amersham Biosciences) in TBST with 3% BSA. The membrane was again washed with TBST (4 × 10 min each) and developed with a luminol/hydrogen peroxide mixture (Pierce). To detect the presence of biotinylated gp59, the membrane was incubated with 1:8000 dilution of neutravidin horseradish peroxidase conjugate (Pierce) in TBST with 3% BSA for 1 h at room temperature following the blocking step and then was washed with TBST (4 × 10 min each) and developed with a luminol/hydrogen peroxide mixture (Pierce). Chemiluminescence was detected by BioMax film (Kodak) with typical exposure times of 20−60 s.

The site of thiol−thiol cross-linking was mapped by analyzing the tryptic digest of the cross-linked product between gp59 and gp43(exo-). The mixture of the cross-linking reaction between gp59 and gp43(exo-) was separated on a 6% SDS−PAGE, and the protein bands corresponding to the cross-linked product between gp59 and gp43(exo-) were excised. The gel pieces were then digested with less than 100 ng of trypsin (Sigma, proteomics sequencing grade) in 0.1 M ammonium bicarbonate buffer (pH 8.2) at 37 °C for 15 h. The resulting mixture of peptide fragments was then fractionated with a gradient of 1−95% acetonitrile in 0.15% formic acid in 20 min and then to 90% 2-propanol in

0.15% formic acid in 10 min at a flow rate of 20 μL/min on a HPLC equipped with a Thermo-Hypersil-Keystone BetaBasic C4 column (0.32 × 100 mm). Each fraction was then analyzed by matrix-assisted laser desorption/ionization−time-of-flight (MALDI−TOF) mass spectrometry as described previously (*31*).

Modeling the Complex between gp43 and gp59. X-ray crystallographic coordinates for gp59 were obtained from the RCSB Protein Data Bank. The structure of gp43 in apo, editing, or pol mode was generated individually based on the crystal structure of RB69 polymerase (*41*−*43*) in the corresponding mode respectively using the Swiss PDB-Viewer Homology Modeling Module, and the missing residues were modeled using the Swiss PDBViewer. A series of preliminary protein interaction models between gp59 and all three modes of gp43 were generated by docking the structure of gp43 in each mode and the structure of gp59 using the ClusPro program (http://nrc.bu.edu/cluster/) (*44*). The most favorable preliminary model was checked against the available information, including distances between certain residues of gp43 and gp59 that had been obtained from the cross-linking and FRET experiments.

RESULTS

Inhibition of gp43 Polymerase Activity by gp59 on a Forked DNA. A functional assay of polymerase activity was employed in the format of a primer elongation reaction (strand displacement) on a small forked DNA substrate (34/62/25-mer) (Figure 1A). It was advantageous to use a small forked DNA substrate where strand displacement could be measured accurately without the need to involve additional proteins such as accessory proteins (gp45 and gp44/62) and single-stranded binding protein (gp32), therefore simplifying the interpretation of the experimental results. Furthermore, the binding site of each protein on such a DNA substrate could be easily identified, because gp59 has its highest binding affinity toward the fork region of the DNA (*17*, *45*), whereas gp43 binds preferably at the primer−template junction of duplex DNA (P−T junction). The lagging strand of this forked DNA is a 7-nucleotide single-stranded flap that is sufficient to allow stable binding of gp59 to the fork region (*12*, *17*) but short enough to discourage binding of gp43 to the lagging-strand template. To allow the binding of both gp43 and gp59 on the forked DNA to reach equilibrium during the preincubation, gp43(exo-) was used in this study because it is capable of carrying out a strand-displacement reaction on a small forked DNA substrate but lacks the ability to hydrolyze the primer strand of the DNA substrate.

A slightly excess amount of gp43(exo-) (150 nM) was used to ensure that all of the P−T junctions of the forked DNA (100 nM) were occupied by gp43 in the titration. At each concentration of gp59, the ternary complex of gp43(exo-), gp59, and the forked DNA was allowed to reach binding equilibrium (5 min) before the elongation reaction was initiated by the addition of dNTPs. The progress of each reaction was determined by quantifying the amount of elongated primer, which was calculated from the difference between the amount of the initial primer and the amount of the remaining primer. As depicted in Figure 1B, the amount of elongated primer in each reaction decreases as the concentration of gp59 increases, demonstrating an inhibition of gp43 activity by gp59. The inhibition of primer elongation follows a sigmoidal curve (Figure 1C), generated by fitting the data with a dose−response equation described in the Materials and Methods. The inhibition curve reaches a plateau when the concentration of gp59 is above 1.5 μM in

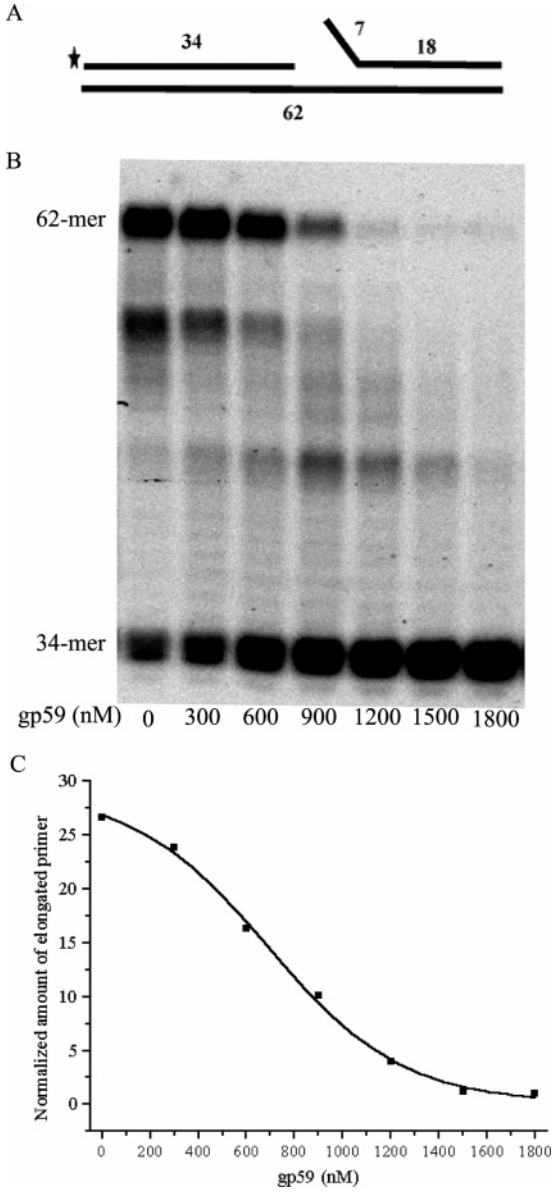

FIGURE 1: Inhibition of gp43 polymerase activity by gp59 on the forked DNA substrate. (A) Diagram of a small forked DNA substrate with a 7-nucleotide single-stranded flap used in the strand-displacement reaction. The ^{32}P label is represented by a star at the 5′ end of the primer strand. (B) Results of strand-displacement reactions by gp43(exo-) in the presence of various concentrations of gp59 as described in the Materials and Methods. ^{32}P-labeled 34-mer primers and ^{32}P-labeled 62-mer products of the strand-displacement reaction on a 12% denaturing polyacrylamide gel are shown. (C) Titration curve describes the relationship between the progress of the reaction determined by the amount of elongated primer and the concentration of gp59. The amount of elongated primer in each reaction was calculated from the difference between the amount of the initial primer and the amount of remaining primer and was normalized to an arbitrary number. The amount of elongated primer in each reaction decreases as the concentration of gp59 increases. The inhibition of primer elongation reaches a plateau when the concentration of gp59 is above 1.5 μM (EC_{50} = 790 ± 60 nM, and n = 2.5).

accordance with an $EC_{50} = 790 \pm 60$ nM, the concentration of gp59 required to achieve the inhibition of half of the gp43 activity, and a Hill coefficient of $n = 2.5$. A simple one-site binding model failed to provide a reasonable fit for the resulting data, and we did not pursue any further data fitting with more rigorous equations. The additional complexity probably arises from the binding of multiple gp59 proteins to the DNA substrate, and the concentration of unbound gp59 is not known. Moreover, we used four different measures (*vide infra*) of the interaction of gp59 with gp43; therefore, it is conceivable that the oligomeric state of gp59 encountered differs, resulting in a range of *n* values. The reported *n* values should not be viewed as rigorously indicative of gp59 binding stoichiometry in the absence of further data.

Formation of the gp43−gp59 Complex on a Forked DNA Substrate Monitored by FRET. The FRET between OG-gp43(exo-) and CPM-gp59 in the presence of a forked DNA substrate has been reported previously (*31*) and is a strong indication of the close contact between the two proteins (less than 100 Å) owing to their complex formation on the DNA. Because we believe that the inhibition of gp43 activity by gp59 is due to their interaction on the DNA, we sought to verify our hypothesis by carrying out an equilibrium FRET titration experiment under the same condition where the inhibition of gp43 activity by gp59 was observed. Our objective was to establish a correlation between the extent of inhibition of gp43 activity by gp59 and the level of the gp43−gp59 complex formed.

At each concentration of CPM-gp59(C42A), measurements were taken both in the presence and absence of the forked DNA substrate (34/62/25-mer). In the absence of DNA, the background FRET observed between N-terminal-labeled OG-gp43(exo-) and CPM-gp59(C42A) resulted mainly from a nonspecific interaction between the two proteins. The difference in the FRET signal between OG-gp43(exo-) and CPM-gp59(C42A) in the presence and absence of DNA provided a titration curve (Figure 2) as a function of the concentration of CPM-gp59(C42A).

The resulting titration curve (Figure 2) shows that the FRET signal between gp43 and gp59 increases as the concentration of gp59 increases, suggesting a gp59 concentration dependence for the amount of the protein complex formed between gp43 and gp59 on the DNA. The formation of the complex reaches a plateau when the concentration of gp59 is above 1.5 μM; presumably all of the gp43 on the P−T junction of DNA has complexed to gp59 at this concentration ($EC_{50} = 540 \pm 50$ nM, and $n = 2.2$). Considering the similar behavior noted in Figure 1C and Figure 2, it is reasonable to conclude that the inhibition of gp43 activity is due to its complex formation with gp59 on the DNA. This argues against the possibility that the inhibition of gp43 activity by gp59 is caused by a competitive binding between gp59 and gp43 to the P−T junction of the DNA substrate, in which case a decrease in the amount of the protein complex formed between gp43 and gp59 would be expected as the concentration of gp59 increases. Our result is consistent with a previous report (*17*) that gp59 does not form stable complexes with single-stranded DNA shorter than a 40-mer or a duplex DNA shorter than a 35-mer. Interestingly, FRET signals in the presence of DNA vary insignificantly when the single-stranded gap on the leading strand was shortened from 10 nucleotides to 6 or 2 nucleotides (data not shown). Therefore, short distances between the 3′ OH of the primer and the duplex region of the fork do not affect the abilities of both gp59 and gp43 to bind simultaneously and form a complex on the fork.

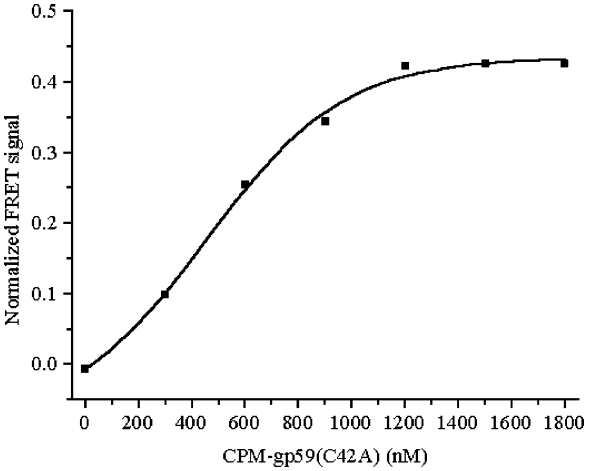

FIGURE 2: Titration of OG-gp43(exo-) by CPM-gp59(C42A) on the forked DNA monitored by FRET. An equilibrium FRET titration experiment was carried out between OG-gp43(exo-) and CPM-gp59(C42A) under the same condition at which the inhibition of gp43 activity by gp59 was observed. The titration curve as a function of the concentration of CPM-gp59(C42A) was obtained by comparing the difference in the FRET signals in the presence and absence of the forked DNA. The resulting FRET signals were normalized to an arbitrary value. The resulting titration curve suggests a gp59 concentration dependence for the amount of the protein complex formed between gp43 and gp59 on the DNA. The formation of such a complex reaches a plateau when the concentration of gp59 is above 1.5 μM ($EC_{50} = 540 \pm 50$ nM, and $n = 2.2$).

Gp59 Binds to the Fork Region and Protects Against RsaI Digestion. The duplex region of the forked DNA substrate (34/62/50-mer) contains an *Rsa*I site (5′-GTAC-3′) that is 8 nucleotides away from the single-stranded region of the fork (Figure 3A). Because gp59 exhibits a binding site of 8−10 nucleotides (*32*), its association at the fork region should prevent access of *Rsa*I, thus protecting the fork from *Rsa*I digestion.

In the absence of gp59, *Rsa*I was able to cut the duplex region of the forked DNA to produce a 40-mer fragment (Figure 3B), indicating that gp43 was likely bound to the P−T junction of the leading-strand DNA. As the concentration of gp59 increased, less digestion product was observed as a result of protection by the binding of gp59. When the concentration of gp59 reached above 1.5 μM, quantitative complex formation between gp43 and gp59 likely occurred on the DNA concomitant with minimal cleavage by *Rsa*I (Figure 3C, $EC_{50} = 880 \pm 20$ nM, and $n = 5.5$). This experiment therefore demonstrates that gp59 remained bound to the forked region of the DNA substrate when complexed with gp43.

Wild-Type gp43 3′ → 5′ Exonuclease Activity Inhibited by gp59 on a Forked DNA. Wild-type gp43 presents a 3′ → 5′ exonuclease activity, which is capable of hydrolyzing the primer strand 3′ → 5′ in the absence of dNTPs. The exonuclease activity of wild-type gp43 at each concentration of gp59 was measured by incubating gp59 with the 34/62/25-mer forked DNA (100 nM), then adding wild-type gp43 (150 nM) to each reaction mixture, and finally quantifying the amount of remaining intact primer after incubation for

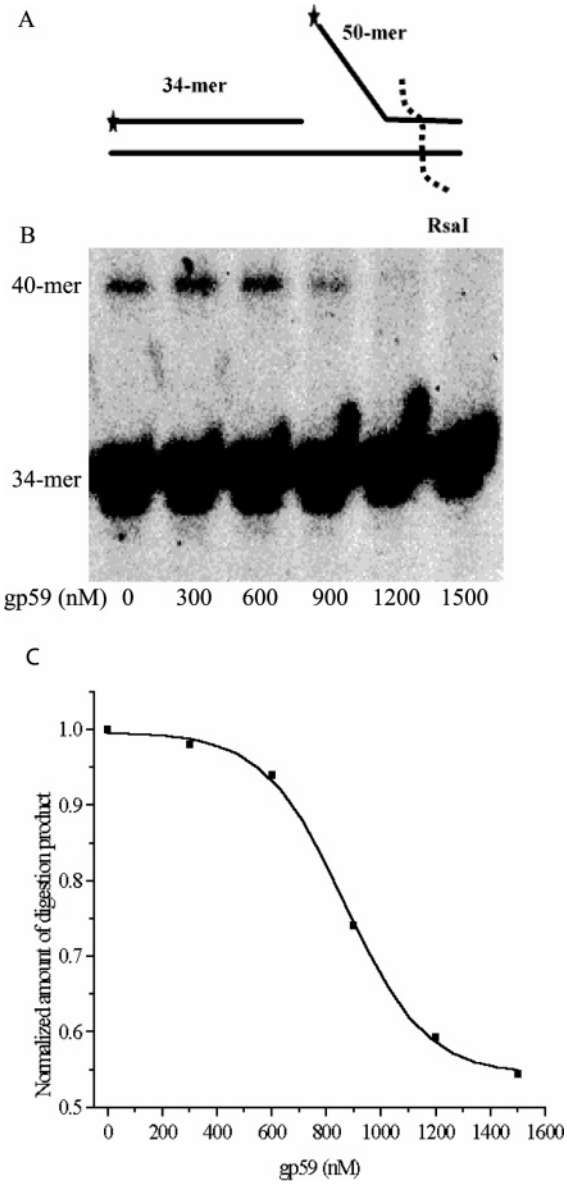

FIGURE 3: Protection of the forked DNA against *Rsa*I digestion. (A) Diagram of the forked DNA substrate with ^{32}P-labeled 34-mer primers and ^{32}P-labeled 50-mer lagging strand containing a 32-nucleotide single-stranded flap used in the *Rsa*I digestion reaction. The *Rsa*I site is 8 nucleotides away from the branch region of the fork. The ^{32}P labels are represented by stars at the 5′ end of both strands. (B) Results of digestion reactions by *Rsa*I in the presence of various concentrations of gp59 and 150 nM of gp43(exo-), as described in the Materials and Methods. ^{32}P-labeled 34-mer primers and ^{32}P-labeled 40-mer products of *Rsa*I digestion reactions on a denatured PAGE are shown. (C) Titration curve describes the relationship between the amount of *Rsa*I digestion product and the concentration of gp59. The amount of digestion product in each reaction is normalized to the amount of digestion product in the absence of gp59. As the concentration of gp59 increases, less digestion product is observed as a result of protection by the binding of gp59. The minimal cleavage by *Rsa*I is shown when the concentration of gp59 reaches 1.5 μM (EC_{50} = 880 ± 20 nM, and n = 5.5).

30 s. As depicted in Figure 4A, the amount of hydrolyzed primer in each reaction decreases as the concentration of gp59 increases and shows an inhibition titration curve (Figure 4B, EC_{50} = 582 ± 0 nM, and n = 4.0) similar to that for the inhibition of polymerase activity (Figure 1C). If the interaction between gp43 and gp59 simply represents the

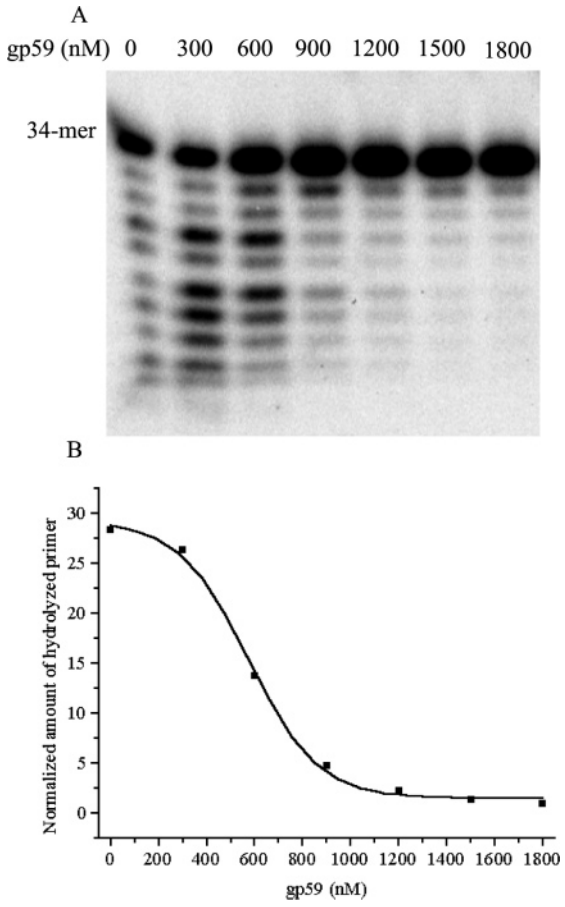

FIGURE 4: Inhibition of wild-type gp43 3′ → 5′ exonuclease activity by gp59 on the forked DNA substrate. (A) Results of wild-type gp43 exonuclease digestion on the 34/62/25-mer DNA substrate in the presence of various concentrations of gp59. The 34-mer primer strand was labeled with ^{32}P phosphate at its 5′ end, represented by a star at its 5′ end. The labeled primers and the digestion products are shown on a denatured PAGE. (B) Titration curve describes the relationship between wild-type gp43 exonuclease activity and the concentration of gp59. The amount of hydrolyzed primer in each reaction was calculated from the difference between the amount of the initial primer and the amount of remaining primer and was normalized to an arbitrary number. The amount of the hydrolyzed primer decreases as the concentration of gp59 increases and shows an inhibition titration curve (EC_{50} = 580 ± 0 nM, and n = 4.0) similar to that for the polymerase activity.

juxtaposition of the two proteins within the confines of the replication fork, we would not expect inhibition of the exonuclease activity, given gp43 moving away from the fork. Therefore, it is highly likely that the inhibition of polymerase activity by gp59 is due to a specific contact between these two proteins rather than simply a steric block.

gp43 Polymerase Activity Inhibited by gp59 as Observed by Single-Molecule FRET. The functional properties of the gp43−gp59 complex were demonstrated by single-molecule fluorescence microscopy that measured FRET on single-forked DNA molecules (34/62/bio50-mer), whose 3′-lagging-strand (50-mer) ends were immobilized on a microscope glass slide through biotin−avidin chemistry (Figure 5A). The presence of gp43 bound to each forked DNA molecule was displayed in Figure 5B as a bright dot in a with filter set 1 (F1), designed for detection of a donor fluorophore such as A488, when an A488-labeled gp43(exo-) was bound. There was no bright dot visible in b and c, because filter 3 (F3)

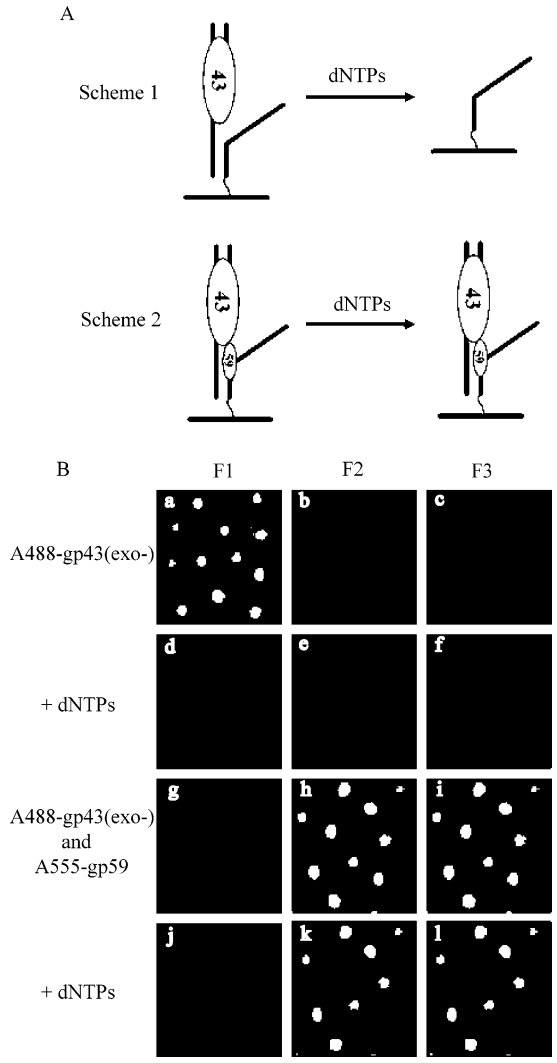

FIGURE 5: Inhibition of gp43 polymerase activity by gp59 as observed by single-molecule FRET. (A) Reaction schemes of the functional properties of the gp43−gp59 complex observed by single-molecule fluorescence microscopy. The reactant and the product in Scheme 1 are represented by a−c and d−f, respectively; the reactant and the product in Scheme 2 are represented by g−i and j−l, respectively. (B) Results of observed single-molecule FRET on a set of immobilized single-forked DNA molecules. The microscope filters were set to observe fluorescence from three different sources: F1, emission from donor A488 (excitation at 488 nm/emission at 510−540 nm); F2, emission from energy transfer between A488 and A555 (excitation at 488 nm/emission at 595−645 nm); and F3, emission from acceptor A555 (excitation at 514 nm/emission at 535−585 nm). dNTPs (100 μM) were present during the measurements displayed in d−f and j−l.

was designed for detection of an acceptor fluorophore such as A555 and filter 2 (F2) was designed for the detection of FRET between the donor/acceptor pairs.

When 100 μM dNTPs were introduced into the mixture of labeled gp43(exo-) bound to the forked DNA, the bright spots of labeled gp43(exo-) shown in a disappeared (F1, d), documenting the dissociation of gp43 from the immobilized DNA, most likely by dissociation of newly synthesized duplex from the anchoring strand as diagramed in Scheme 1 of Figure 5A. This result is consistent with the activity of unlabeled gp43(exo-) demonstrated in the above ensemble experiments, validating the activity of the labeled polymerase on the immobilized DNA required by the single-molecule experiments and establishing the biological relevance of the experimental setup.

In the second set of single-molecule experiments (g−l), both the A488-labeled gp43(exo-) and the A555-labeled gp59 were able to bind to the forked DNA molecules. The binding of the A555-labeled gp59 on the forked DNA molecules was displayed as the bright dots in i by F3. In h, the FRET was detected by F2 as the light emitted from the A555 on gp59, resulting from energy transfer from the A488 on gp43(exo-) to the A555 on gp59. The detection of the FRET between A488 and A555 (R_0 = 70 Å) implies intimate protein−protein contacts between gp43 and gp59 on the forked DNA. The binding of the A488-labeled gp43(exo-) was not observed by F1 (g) because of the complete quenching of the fluorophore A488. When dNTPs were added to the observation cell containing the ternary complex of gp43(exo-). gp59, and the forked DNA, most of the FRET spots remained (80%), indicating that the DNA-bound gp43(exo-) was no longer capable of catalyzing nucleotide incorporation causing subsequent duplex separation by translocation as a result of inhibition by gp59. A few of the bright dots disappeared in both k and l, because of the protein loss during the handling.

gp43 Polymerase Activity Inhibited by gp59 on a TRFII M13 DNA Substrate. Strand-displacement DNA synthesis was performed on a TRFII M13 DNA substrate (Figure 6A) in the presence of holoenzyme and gp32, which is a closer mimic of the helicase-independent leading-strand synthesis. The extension of the leading-strand primer from an initial size of 7.2 kb was revealed by the incorporation of radiolabeled ^{32}P-dCTP, after separation of the extension reaction products by alkaline agarose gel electrophoresis. As shown in Figure 6B, forks in the absence of gp59 displayed a continuous progression at a calculated rate of 4.9 nucleotide/s with the size of the final leading-strand product up to 9.7 kb after 8 min reaction time, while the progression of the forks in the presence of gp59, which was introduced 1 min after the initiation of the reaction, was mostly stalled at a leading-strand length of 7.7 kb and showed very little change over the same period of time (parts B and C of Figure 6). The stalling of the resulting replication forks demonstrated that gp59 is capable of trapping gp43 at a moving fork, by forming a very stable ternary complex with gp43. The time for gp59 to locate and bind moving forks would be approximately 19 s by establishing the time for the forks to progress from 7.6 kb when gp59 was introduced to 7.7 kb when the majority of the forks were stalled. It is unlikely that the trapping, however, results from gp43 dissociation from the fork followed by fork capture by gp59, given a $t_{1/2} \approx 7$ min for the rate of dissociation of the polymerase from the holoenzyme on the DNA (*40*), compared to a shut-down of replication that occurs within 1 min. In contrast to the total inhibition observed at a static fork (data not shown), when gp59 was added before the initiation of strand-displacement reaction by the addition of dNTPs, a very small number of forks remained active after the addition of gp59 to the moving forks, indicated by the faint faster moving bands on the gel. This likely resulted from some incomplete trapping of moving forks by gp59.

Mapping the Interaction Sites between gp43 and gp59. To have a better understanding of the nature of the contacts between gp43 and gp59, we exploited our earlier finding

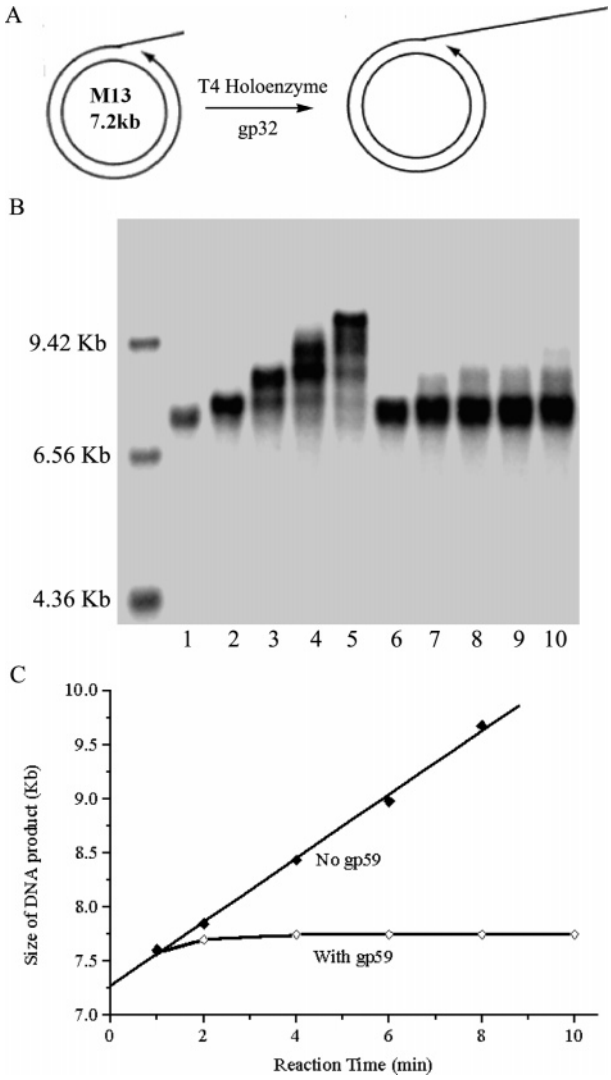

FIGURE 6: Inhibition of gp43 polymerase activity by gp59 on a large DNA substrate. (A) Diagram of strand-displacement reaction using a TRFII M13 DNA substrate. (B) Results of the extension of the leading strand primer by the incorporation of radiolabeled ^{32}P-dCTP are shown on an alkaline agarose gel. For the reactions in lanes 1−5 (absence of gp59), the holoenzyme was allowed to be assembled onto the DNA at 37 °C for 30 s, followed by the addition of gp32. The mixture was incubated at 37 °C for an additional 2.5 min, and the reaction was initiated with the addition of dNTPs. Reaction aliquots were withdrawn at 1, 2, 4, 6, and 8 min. For the reactions in lanes 6−10 (presence of gp59) the reactions were set up the same as the reactions 1−5, except gp59 was added 1 min after the initiation of the reaction. Reaction aliquots were withdrawn at 2, 4, 6, 8, and 10 min after the addition of dNTPs. Forks in the absence of gp59 displayed a continuous progression with the size of the final product up to 9.5 kb, while the progression of the forks in the presence of gp59 was mostly stalled at 7.7 kb and showed very little change over the same period of time. (C) Size of leading-strand DNA synthesis determined in B is plotted as a function of the reaction time. A fork rate of 4.9 nucleotide/s is derived from a linear fit ($Y = 7.27 + 0.294X$) of the plot for the reaction in the absence of gp59.

that the two proteins could be chemically cross-linked in the presence of DNA (*31*). In the presence of the forked DNA substrate (34/62/50-mer), a site-specific chemical cross-linker, BMH, was found suitable for cross-linking gp59 to gp43(exo-), producing a new band corresponding to the size of gp43(exo-) plus gp59 on a denaturing polyacrylamide gel (Figure 7). The same band was not present in the absence

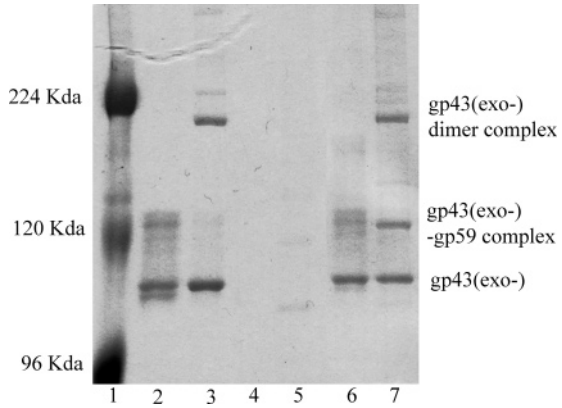

FIGURE 7: Mapping the interaction sites between gp43 and gp59. Detection by Coomassie Brilliant Blue of the cross-linked product between gp43(exo-) and gp59 by a specific chemical cross-linker, BMH, on a 6% denaturing polyacrylamide gel is shown. Lane 1, MW marker; lane2, gp43(exo-) alone; lane 3, gp43(exo-) and the forked DNA; lane 4, gp59 alone; lane 5, gp59 and the forked DNA; lane 6, gp43(exo-) and gp59; lane 7, gp43(exo-), gp59, and the forked DNA. All of the reactions contained BMH.

of the DNA substrate, indicating that this protein complex was formed only on the DNA. The composition of this band was verified by a "double tag" method, in which the biotinylated gp59 and gp43 were detected in the cross-linked product by Western blotting analysis, respectively (data not shown).

To map the site of interaction between gp43 and gp59, an in-gel digestion first was carried out on the cross-linked product of gp43(exo-)−gp59, and the resulting peptide fragments then were separated on a microscale HPLC and analyzed by MALDI−TOF mass spectrometry in a linear mode. As controls, similar experiments were also performed on the individual gp43(exo-) and gp59 proteins. A candidate peak for a cross-linked fragment ($[M + H]^+ = 4376.9$) was identified based on its unique size and by comparison to the fragments generated in control experiments. Because BMH is a homobifunctional cross-linker and is very selective toward sulfhydryl groups under the conditions used for cross-linking, the sites captured by cross-linking are very likely 1 of the 2 cysteines of gp59 and 1 of the 14 cysteines of gp43. Using mutant gp59 proteins (C42A and C215A), we found that only C42A protein cross-links to gp43, thus eliminating Cys42 of gp59 as the attachment site of the cross-linker (data not shown). Therefore, only fragments containing Cys215 of gp59 were considered for matching fragments generated from the amino acid sequences of gp59 and gp43 to the above candidate. Overall, the best match to this candidate fragment was a fragment $[M + H]^+ = 4378.0$ that corresponds to a BMH-cross-linked peptide between Cys169 of gp43 and Cys215 of gp59. From the modeled structure of gp43 derived from the homologous polymerase of RB69, Cys169 is well exposed to the solvent and therefore it is potentially accessible for cross-linking to Cys215 of gp59.

Interaction between gp59 and gp43 Based on Structural Modeling. We generated a series of preliminary protein interaction models between gp59 and gp43 by docking the homology-modeled individual structure of gp43 in the editing, pol, or apo mode with the structure of gp59 using ClusPro, a web-server-based program (http://nrc.bu.edu/cluster/). The structure of gp43 in each apo, editing, or pol mode was generated individually based on the crystal

structure of RB69 polymerase (*41*−*43*) in the corresponding mode respectively using the Swiss PDBViewer Homology Modeling Module. The amino acid sequence of T4 gp43 is 63% identical to that of its homologue the RB69 DNA polymerase (gp43), which shares a similar primary structure to several other pol α family DNA polymerases (*43*). The ClusPro program employs an automated rigid-body docking and discrimination algorithm that rapidly filters docked conformations and ranks them based on their clustering properties, including desolvation and electrostatic energies (*44*). Because the N-terminal domain of gp59 does not interact with gp43 when it is bound to the duplex region of the replication fork and points away from gp43 (*12*), only the C-terminal region of gp59 was used for docking.

Among the three structural modes of gp43, the structure of the editing mode was generated by cocrystallizing gp43 with the primer−template DNA duplex in the absence of dNTP (*42*), whereas the structure of the pol mode was determined with the incoming dTTP bound in the polymerization active site of gp43 (*41*) and the apo mode of gp43 had no DNA bound (*43*). Therefore, the structure of the editing mode of gp43, where the 3′ OH of the primer strand is found in the exonuclease active site of gp43, is undoubtedly the best representation of the static interaction between gp43 and the primer−template DNA duplex for all of our binding studies, even though it has not been established whether the editing mode is the only mode present when gp43 binds to the P−T junction of the DNA duplex.

We evaluated the top 30 results of preliminary models involving the editing mode of gp43 according to the distance information between gp43 and gp59 obtained through cross-linking and FRET experiments. On the basis of the fact that cross-linking was achieved between Cys215 of gp59 and Cys169 of gp43 on the forked DNA by using the linker BMDB with a spacer of 10.2 Å (data not shown), the spatial distance between these two cysteines should be within 10.2 Å. Also on the basis of the FRET efficiency measured between the CPM-labeled gp59 (C42A) and the OG-labeled gp43(exo-) (R_0 = 48 Å), the distance between Cys215 of gp59 and the N terminus of gp43 was estimated to be 50 Å. This information reduced the preliminary models to the gp59−gp43 complex model shown in Figure 8A, with a distance of 7.9 Å between the two cross-linked cysteine residues (Figure 8D) and a distance of 55 Å between the N terminus of gp43 and Cys215 of gp59, which was in a close agreement to the experimental values (50 Å), considering the uncertainty introduced by the flexibility of the N terminus of gp43. This current model also has a reasonable alignment between gp59 and gp43 that will likely allow the forked DNA to bind both proteins simultaneously without too many twists and turns.

As displayed in our interaction model (parts A and B of Figure 8), the gp59 inserts both its C-terminal α-helix H13 (Gln202-Lys217) and loop H7−H8 (Lys126-Glu134) into a prominent wedge-shaped cleft between the exonuclease domain and the thumb domain of gp43, where the residues in the C-terminal α-helix H13 make extensive contacts with the exonuclease domain of gp43 and the residues in the loop H7−H8 interact with the residues on the inner surface of the thumb domain. Besides the topological match between the two protein interfaces (Figure 8B), numerous residues are found to be capable of forming up to seven pair of hydrogen bonds between the interfaces of the two proteins. Furthermore, both the gp59 C-terminal α helix and the loop H7−H8 contain several hydrophobic residue/patches on the outer surface, such as Val207, Ile209, and Val129, where all of these hydrophobic residues are buried between the protein interfaces and excluded from the solvent. Among them, Val207 and Ile209 of the α-helix H13 in particular, make contacts with hydrophobic patches on the gp43 surface, where Val207 interacts with Leu163, and Ile209 contacts Leu300, Pro301, and Tyr320. These hydrogen bonds and hydrophobic interactions collectively drive the complex formation between gp43 and gp59.

Another interesting facet of the model is the orientation of the side chain of Cys215 of gp59 that cross-links gp59 and gp43 with the thiol-reactive homobifunctional cross-linkers BMH and BMDB. On the basis of our structural model, although the C-terminal helix of gp59 makes extensive contacts with gp43, the sulfhydryl group of Cys215 of gp59 protrudes away from the buried protein interface and is properly oriented toward the Cys169 in the exonuclease domain of gp43 for cross-linking. This is also consistent with the fact that labeling Cys215 of gp59 with a bulky fluorescent dye molecule did not disrupt the specific interaction between gp43 and gp59 as probed by FRET.

We also assessed the top 30 preliminary models involving the pol mode of gp43. None of the resulting complexes showed the same kind of interaction between the C-terminal domain of gp59 and the exonuclease and thumb domain of gp43 that has often been observed in the models generated with the editing mode of gp43. We noted that the cleft between the exonuclease domain and the thumb domain of gp43 appears to close up when the editing mode of gp43 switches to the pol mode and the newly formed surfaces between the two domains are apparently incapable of interacting with the C-terminal domain of gp59 (Figure 8C). This implies that gp59 may not interact with the pol mode of gp43 and may only trap gp43 by insertion when gp43 switches to the editing mode.

DISCUSSION

The recruiting and loading of gp41 at replication forks, created within D loops by invasion and annealing of a single-stranded 3′ end of T4 DNA to a homologous region is a universal step in replisome assembly during recombination-dependent replication (*23*). The helicase loader gp59 is required to accomplish this task. Gp59 has a high affinity toward forked DNA substrates such as D and R loops (*12*, *17*, *20*) and interacts with multiple proteins, such as gp32 and gp41 (*17*, *46*, *47*). These properties allow gp59 to recognize the specific structure of forked DNA where the displaced strand is coated with gp32 and to load gp41 onto the strand.

Besides loading helicase, the role of gp59 in promoting homologous recombination-dependent DNA replication during T4 development is still unclear. It has been proposed that gp59 helps coordinate the initiation of leading- and lagging-strand DNA synthesis by inhibiting leading-strand synthesis by the holoenzyme before the helicase gp41 is loaded, based on observations from replication reactions involving gp43 on the leading strand using a variety of DNA substrates, such as a preformed R loop (*20*), a forked M13

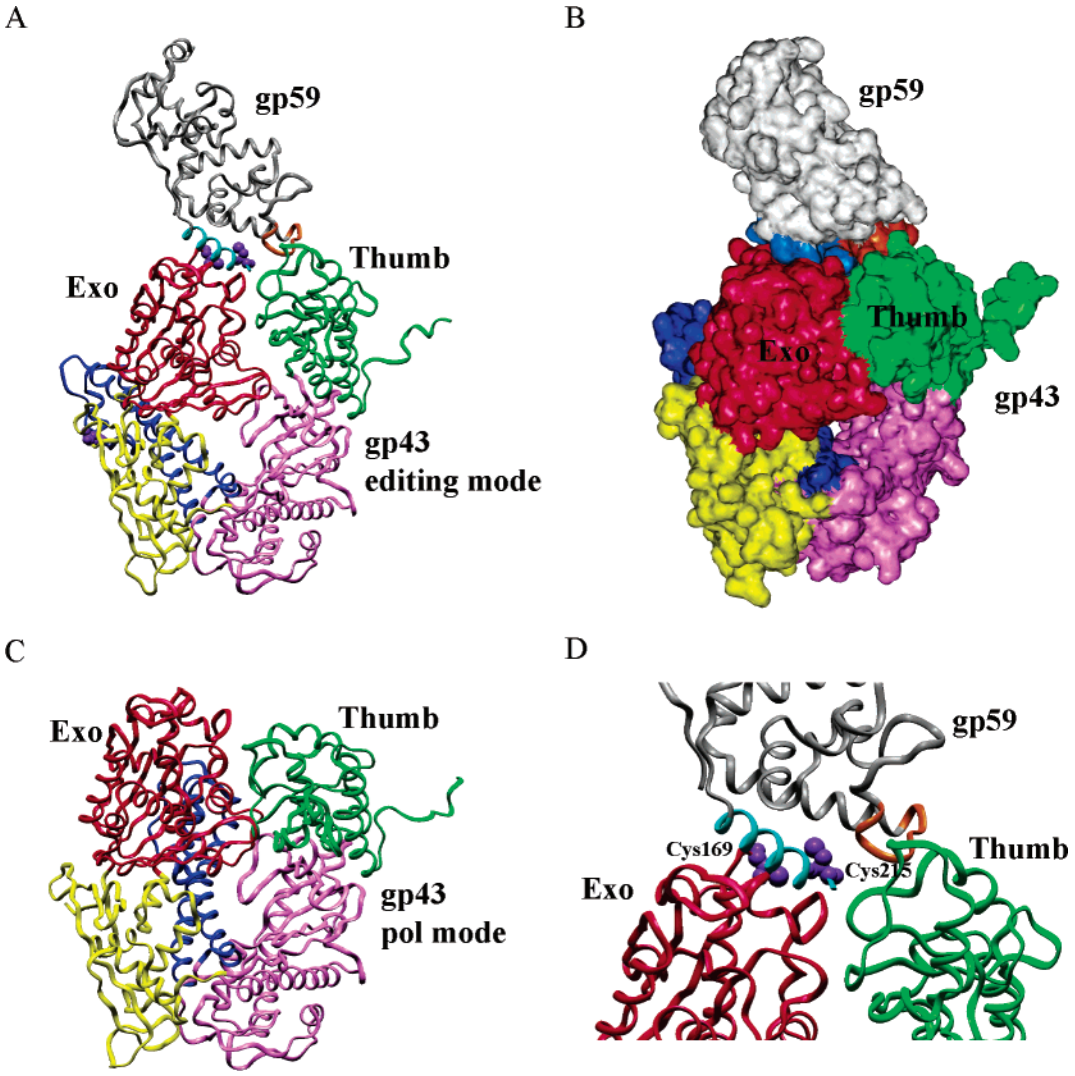

FIGURE 8: Interaction between gp59 and gp43 based on structural modeling. (A) Protein interaction model between gp59 and gp43 in the editing mode, shown in a ribbon representation, is colored as follows: for gp43, the N-terminal domain (residues 1−108 and 340−382) is in yellow, the exonuclease domain (residues 109−339) is in red, palm (residues 383−468 and 573−729) is in magenta, fingers (residues 469−572) are in blue, and thumb (residues 730−898) is in green; for gp59, C-terminal α-helix H13 (Gln202-Lys217) is in cyan and loop H7−H8 (Lys126 to Glu134) is in gold, the rest of gp59 is in gray. The Cys169 and Met1 of gp43 and Cys215 of gp59 are in CPK representation and are colored purple. The distance between Cys169 of gp43 and Cys215 of gp59 is 7.9 Å. The distance between Met1 of gp43 and Cys215 of gp59 is 55 Å. (B) Protein interaction model between gp59 and gp43 in the editing mode, shown in a solid 3D representation, follows the identical color scheme as in A. (C) Protein model of gp43 in the pol mode, shown as ribbon representation, follows the identical color scheme as in A. (D) Close-up view of gp43- and gp59-docking interface. The ribbons are colored according to the scheme in A. The Cys215 in gp59 and Cys169 in gp43 are shown as a CPK model and labeled.

DNA (*21*), or a nicked double-stranded M13 (*32*). Given the fact that gp43 interacts with gp59 on a replication fork, the inhibition of polymerization by gp59 was attributed to the blockage of the forward movement of the leading-strand polymerase gp43 by the DNA-bound gp59 (*16*, *21*).

We tested this hypothesis by employing a simple replication model system with a minimum number of necessary components including gp43(exo-), gp59, and a small forked DNA substrate. Our experimental results showed that the amount of replicative extension of the primed fork decreased as the concentration of gp59 increased, indicating that gp59 was capable of shutting down the polymerization activity of gp43 on the leading strand. We attribute the inhibition of gp43 activity by gp59 to trapping of gp43 through a complex formed between gp43 and gp59 on the DNA. This was unambiguously demonstrated by single-molecule FRET microscopy, which established that when the A555-labeled gp59 and the A488-labeled gp43(exo-) were within contact distance, the activity of the A488-labeled gp43(exo-) was inhibited.

We also followed the formation of such a complex on the forked DNA by monitoring the FRET signal between the CPM-labeled gp59(C42A) and the OG-labeled gp43(exo-). The degree of inhibition of gp43 polymerase activity by gp59 as well as the amount of gp43−gp59 complex formation followed the same dependence on gp59 concentration and thus verified that the inhibition of gp43 activity by gp59 was due to the trapping of gp43 by complex formation between the two proteins on the DNA. The protection by the gp43−gp59 complex against *Rsa*I digestion of the forked DNA substrate also showed a similar dependence on gp59 levels. We thus excluded an alternative inhibition mechanism, in which competitive binding between gp43 and gp59 might prevent the access of gp43 to the P−T junction on the leading

strand of the forked DNA substrate, a model which had been proposed for the inhibition of leading-strand polymerase activity by PriA (an *E. coli* gp59 homologue) on a D loop (*48*, *49*).

To investigate whether inhibition of the leading strand synthesis by gp59 extended to a more complex model system, we carried out helicase-independent leading-strand synthesis with additional replication proteins (gp32, gp45, and gp44/62) on a forked M13 substrate. While the replication forks in the absence of gp59 displayed progressive DNA synthesis, most of the forks in the presence of gp59, which was introduced 1 min after the initiation of the reaction, were stalled and showed very little DNA synthesis over the next 8 min. Thus, the inhibition of gp43 activity by gp59 is nearly complete and provides a relatively static replication fork to continue the assembly of the replisome.

We have demonstrated that gp59 is capable of binding to both moving and static replication forks. This may be interpreted to suggest that the assembly of the holoenzyme may conceivably precede the binding of gp59 to the fork, which is likely associated with helicase-independent bubble migration during the initiation of recombination-dependent replication. However, we have also shown that gp59 binding to active forks can be less efficient than gp59 binding to static forks, presumably because of the difficulty for gp59 to recognize and bind the constantly changing and moving forked structure driven by the active polymerase. Having gp59 bound to the static forked structure of the D loop prior to the assembly of the leading-strand holoenzyme will likely reduce unproductive helicase-independent bubble migration and therefore seems to be the preferred sequence for initiation of recombination-dependent replication. Moreover, if the 3′ OH of the invading strand is in close vicinity to the forked structure, (the equivalent of a D loop), the proximity of gp59 may assist in the leading-strand holoenzyme assembly by interacting with gp43 on the 3′ OH of the invading strand.

Finally, it is noteworthy that gp59 is capable of inhibiting the exonuclease activity of gp43, preventing the loss of the primer during replisome assembly. This is strong evidence against a steric block model where gp59 simply prevents the forward movement of gp43 during replication and suggests that gp43 and gp59 form a unique complex.

On the basis of the elegant X-ray crystal structure studies of the phage RB69 DNA polymerase, a close homologue of T4 DNA polymerase gp43, and especially the availability of the structures of the polymerase both in an editing (*42*) and pol (*41*) mode, as well as the structure of gp59 (*12*), we were able to create a model of the gp59−gp43 complex by homology modeling constrained by the distance information derived from our cross-linking and FRET data.

We have noted both in our model and in the structure of RB69 polymerase that there is a cleft formed between the thumb and exonuclease domains in the editing mode. Upon switching to the pol mode, the two domains move toward each other and close up the cleft. During the transition of switching, the axis of the duplex DNA bound to one active site of the RB69 DNA polymerase is rotated by 40° relative to its orientation when bound to the other site (*41*). Such reorientation of the DNA, as it traverses back and forth between the polymerase and the exonuclease sites, appears to be guided by the aforementioned conformational change of the thumb domain, which constrains the diffusion of DNA to one dimension between the two sites and accelerates the switching between the pol and editing modes. Interference with the conformational change of the thumb domain will likely affect the primer−template DNA orientation with respect to the two sites and impede both the polymerization and exonuclease activities of the enzyme. This agrees with the results of the mutation studies on RB69 polymerase, where the mutations within the thumb domain have significant impacts on both of the activities of the enzymes (*50*−*53*). Thus, both the polymerization and exonuclease activities could be shut down by gp59, if substrate switching between the two modes of gp43 is inhibited by the interaction between gp59 and gp43.

As displayed in our model of the complex between gp59 and the editing mode of gp43, gp59 inserts both its C-terminal α-helix H13 (Gln202-Lys217) and loop H7−H8 (Lys126-Glu134) into a cleft between the exonuclease domain and the thumb domain of gp43, where the C-terminal α-helix H13 of gp59 makes extensive contact with the exonuclease domain of gp43 and the loop H7−H8 of gp59 interacts with the residues on the inner surface of the thumb domain. The resulting interaction prevents closing of the cleft between the two domains and will retard the dynamic switching of polymerase between the pol and editing modes leading to loss of both polymerase and exonuclease activities. The model further suggests that gp59 most likely interacts with the editing mode of gp43 where the cleft is open rather than with the pol mode of gp43. Consequently, gp59 should be more efficient in trapping a static gp43 where the enzyme may have an easier access to the editing mode rather than the pol mode.

When gp43 is locked in a fixed conformation preventing the dynamic switching between the editing and pol modes, it will be necessary to restore the polymerase activities of the enzyme by attenuating the interaction between gp43 and gp59. The loading of helicase gp41 onto the lagging strand will likely provide the key to unlocking the gp43 and gp59 complex.

In our structural model, only one molecule of gp59 interacts with the leading-strand polymerase gp43 and consequently inhibits the gp43 activity. However, all of the titration curves in our studies are of sigmoidal shape and do not fit well with the simple one-site binding model. This can be rationalized by assuming, while interacting with gp43, gp59 may also form an oligomeric structure bound to the forked DNA and the formation of the gp43−gp59 complex on DNA is dependent on the formation of such an oligomeric structure of gp59. This would result in a sigmoidal binding curve with a possible positive cooperativity. Although a similar sigmoidal binding curve for gp59 has been reported previously (*32*), the nature of this oligomeric structure is still unclear. Because gp59 induces the oligomerization of gp41 (*15*) and the maximum activity of DNA unwinding occurs when gp41 and gp59 are in a 1:1 ratio (*8*), it is conceivable that gp59 may form a hexameric-ring structure like that of gp41.

The inhibition of leading-strand DNA synthesis by a helicase-loading protein is not unique to the T4 replication system. In some other organisms, the helicase-loading proteins or probably other accessory proteins may also exhibit a similar type of activity to promote primosome assembly and coordinate leading- and lagging-strand synthesis by inhibiting the leading-strand synthesis. In *E. coli*, bacterial

PriA protein, whose main function is probably to restart replication after replication fork arrests with the aid of homologous recombination proteins, was found to inhibit leading-strand synthesis (*48*), presumably by regulating the access by the leading-strand polymerase to the 3′ end of the primer within the D loop (*49*), to which PriA binds with high affinity. Because PriA initiates assembly of a more complex primosome in a process requiring up to seven primosome and accessory proteins, such inhibition would be critical to control the timing of the leading-strand synthesis relative to the process of the primosome assembly.

ACKNOWLEDGMENT

We acknowledge Dr. A. Daniel Jones for assistance with the MALDI mass spectrometry analysis and Dr. Scott Nelson for help with the data fitting.

REFERENCES

1. Alberts, B. M. (1987) Prokaryotic DNA replication mechanisms, *Philos. Trans. R. Soc. London, Ser. B 317*, 395−420.
2. Nossal, N. G. (1994) The bacteriophage T4 DNA replication fork, in *Molecular Biology of Bacteriophage* (Karam, J. D., Ed.) pp 43−55, ASM Press, Washington, D.C.
3. Benkovic, S. J., Valentine, A. M., and Salinas, F. (2001) Replisome-mediated DNA replication, *Annu. Rev. Biochem. 70*, 181−208.
4. Capson, T. L., Peliska, J. A., Kaboord, B. F., Frey, M. W., Lively, C., Dahlberg, M., and Benkovic, S. J. (1992) Kinetic characterization of the polymerase and exonuclease activities of the gene 43 protein of bacteriophage T4, *Biochemistry 31*, 10984−10994.
5. Dong, F., Gogl, E. P., and von Hippel, P. H. (1995) The phage T4-coded DNA replication helicase (gp41) forms a hexamer upon activation by nucleoside triphosphate, *J. Biol. Chem. 270*, 7462−7473.
6. Venkatesan, M., Silver, L. L., and Nossal, N. G. (1982) Bacteriophage T4 gene 41 protein, required for the synthesis of RNA primers, is also a DNA helicase, *J. Biol. Chem. 257*, 12426−12434.
7. Barry, J. and Alberts, B. (1994) Purification and characterization of bacteriophage T4 gene 59 protein. A DNA helicase assembly protein involved in DNA replication, *J. Biol. Chem. 269*, 33049−33062.
8. Raney, K. D., Carver, T. E., and Benkovic, S. J. (1996) Stoichiometry and DNA unwinding by the bacteriophage T4 41:59 helicase, *J. Biol. Chem. 271*, 14074−14081.
9. Valentine, A. M., Ishmael, F. T., Shier, V. K., and Benkovic, S. J. (2001) A zinc ribbon protein in DNA replication: Primer synthesis and macromolecular interactions by the bacteriophage T4 primase, *Biochemistry 40*, 15074−15085.
10. Cha, T. A. and Alberts, B. M. (1990) Effects of bacteriophage T4 gene 41 and gene 32 proteins on RNA primer synthesis: Coupling of leading- and lagging-strand DNA synthesis at a replication fork, *Biochemistry 28*, 4374−4382.
11. Bhagwat, M. and Nossal, N. G. (2001) Bacteriophage T4 RNase H removes both RNA primers and adjacent DNA from the 5′ end of lagging strand fragments, *J. Biol. Chem. 276*, 28516−28524.
12. Mueser, T. C., Jones, C. E., Nossal, N. G., and Hyde, C. C. (2000) Bacteriophage T4 gene 59 helicase assembly protein binds replication fork DNA. The 1.45 Å resolution crystal structure reveals a novel α-helical two-domain fold, *J. Mol. Biol 296*, 597−612.
13. Shamoo, Y., Friedman, A. M., Parsons, M. R., Konigsberg, W. H., and Steitz, T. A. (1995) Crystal structure of a replication fork single-stranded DNA binding protein (T4 gp32) complexed to DNA, *Nature 376*, 362−366.
14. Ishmael, F. T., Alley, S. C., and Benkovic, S. J. (2001) Identification and mapping of protein−protein interactions between gp32 and gp59 by cross-linking, *J. Biol. Chem. 276*, 25236−25242.
15. Ishmael, F. T., Alley, S. C., and Benkovic, S. J. (2002) Assembly of the bacteriophage T4 helicase: Architecture and stoichiometry of the gp41−gp59 complex, *J. Biol. Chem 277*, 20555−20562.
16. Jones, C. E., Mueser, T. C., Dudas, K. C., Kreuzer, K. N., and Nossal, N. G. (2001) Bacteriophage T4 gene 41 helicase and gene 59 helicase-loading protein: A versatile couple with roles in replication and recombination, *Proc. Natl. Acad. Sci. U.S.A. 98*, 8312−8318.
17. Jones, C. E., Mueser, T. C., and Nossal, N. G. (2000) Interaction of the bacteriophage T4 gene 59 helicase loading protein and gene 41 helicase with each other and with fork, flap, and cruciform DNA, *J. Biol. Chem. 275*, 27145−27154.
18. Kreuzer, K. N. and Morrical, S. W. (1994) in *Molecular Biology of Bacteriophage T4* (Karem, J. D., Ed.) pp 28−42, American Society for Microbiology, Washington, D.C.
19. Mosig, G. (1998) Recombination and recombination-dependent DNA replication in bacteriophage, *Annu. Rev. Genet. 32*, 379−413.
20. Nossal, N. G., Dudas, K. C., and Kreuzer, K. N. (2001) Bacteriophage T4 proteins replicate plasmids with a preformed R loop at the T4 ori(uvsY) replication origin *in vitro*, *Mol. Cell 7*, 31−41.
21. Jones, C. E., Mueser, T. C., and Nossal, N. G. (2004) Bacteriophage T4 32 protein is required for helicase-dependent leading strand synthesis when the helicase is loaded by the T4 59 helicase-loading protein, *J. Biol. Chem. 279*, 12067−12075.
22. Kong, D., Nossal, N. G., and Richardson, C. C. (1997) Role of the bacteriophage T7 and T4 single-stranded DNA-binding proteins in the formation of joint molecules and DNA helicase-catalyzed polar branch migration, *J. Biol. Chem. 272*, 8380−8387.
23. Bleuit, J. S., Xu, H., Ma, Y., Wang, T., Liu, J., and Morrical, S. W. (2001) Mediator proteins orchestrate enzyme−ssDNA assembly during T4 recombination-dependent DNA replication and repair, *Proc. Natl. Acad. Sci. U.S.A. 98*, 8298−8305.
24. Spacciapoli, P. and Nossal, N. G. (1994) Interaction of DNA polymerase and DNA helicase within the bacteriophage T4 DNA replication complex. Leading strand synthesis by the T4 DNA polymerase mutant A737V (tsL141) requires the T4 gene 59 helicase assembly protein, *J. Biol. Chem. 269*, 447−455.
25. Delagoutte, E. and von Hippel, P. H. (2001) Molecular mechanisms of the functional coupling of the helicase (gp41) and polymerase (gp43) of bacteriophage T4 within the DNA replication fork, *Biochemistry 40*, 4459−4477.
26. Dong, F., Weitzel, S. E., and von Hippel, P. H. (1996) A coupled complex of T4 DNA replication helicase (gp41) and polymerase (gp43) can perform rapid and processive DNA strand-displacement synthesis, *Proc. Natl. Acad. Sci. U.S.A. 93*, 14456−14461.
27. Schrock, R. D., and Alberts, B. (1996) Processivity of the gene 41 DNA helicase at the bacteriophage T4 DNA replication fork, *J. Biol. Chem. 271*, 16678−16682.
28. Cha, T. A., and Alberts, B. M. (1989) The bacteriophage T4 DNA replication fork. Only DNA helicase is required for leading strand DNA synthesis by the DNA polymerase holoenzyme, *J. Biol. Chem. 264*, 12220−12225.
29. Notarnicola, S. M., Mulcahy, H. L., Lee, J., and Richardson, C. C. (1997) The acidic carboxyl terminus of the bacteriophage T7 gene 4 helicase/primase interacts with T7 DNA polymerase, *J. Biol. Chem. 272*, 18425−18433.
30. Kim, S., Dallman, H. G., McHenry, C. S., and Marians, K. J. (1996) Coupling of a replicative polymerase and helicase: A τ-DnaB interaction mediates rapid replication fork movement, *Cell 84*, 643−650.
31. Ishmael, F. T., Trakselis, M. A., and Benkovic, S. J. (2003) Protein−protein interactions in the bacteriophage T4 replisome. The leading strand holoenzyme is physically linked to the lagging strand holoenzyme and the primosome, *J. Biol. Chem. 278*, 3145−3152.
32. Ma, Y., Wang, T., Villemain, J. L., Giedroc, D. P., and Morrical, S. W. (2004) Dual functions of single-stranded DNA-binding protein in helicase loading at the bacteriophage T4 DNA replication fork, *J. Biol. Chem. 279*, 19035−19045.
33. Frey, M. W., Nossal, N. G., Capson, T. L., and Benkovic, S. J. (1993) Construction and characterization of a bacteriophage T4 DNA polymerase deficient in 3′ → 5′ exonuclease activity, *Proc. Natl. Acad. Sci. U.S.A. 90*, 2579−2583.
34. Rush, J., Lin, T.-C., Quinones, M., Spicer, E. K., Douglas, I., Williams, K. R., and Konigsberg, W. H. (1989) The 44P subunit of the T4 polymerase accessory protein complex catalyzes ATP hydrolysis, *J. Biol. Chem. 264*, 10943−10953.
35. Nossal, N. G. (1979) DNA replication with bacteriophage T4 proteins. Purification of the proteins encoded by T4 genes 41, 45, 44, and 62 using a complementation assay, *J. Biol. Chem. 254*, 6026−6031.

36. Yang, J., Trakselis, M. A., Roccasecca, R. M., and Benkovic, S. J. (2003) The application of a minicircle substrate in the study of the coordinated T4 DNA replication, *J. Biol. Chem. 278*, 49828−49838.
37. Kaboord, B. F. and Benkovic, S. J. (1993) Rapid assembly of the bacteriophage T4 core replication complex on a linear primer/template construct, *Proc. Natl. Acad. Sci. U.S.A. 90*, 10881−10885.
38. Trakselis, M. A., Alley, S. C., Abel-Santos, E., and Benkovic, S. J. (2001) Creating a dynamic picture of the sliding clamp during T4 DNA polymerase holoenzyme assembly by using fluorescence resonance energy transfer, *Proc. Natl. Acad. Sci. U.S.A. 98*, 8368−8375.
39. Rajagopalan, P. T., Zhang, Z., McCourt, L., Dwyer, M., Benkovic, S. J., and Hammes, G. G. (2002) Interaction of dihydrofolate reductase with methotrexate: Ensemble and single-molecule kinetics, *Proc. Natl. Acad. Sci. U.S.A. 99*, 13481−13486.
40. Yang, J., Zhuang, Z., Roccasecca, R. M., Trakselis, M. A., and Benkovic, S. J. (2004) The dynamic processivity of the T4 DNA polymerase during replication, *Proc. Natl. Acad. Sci. U.S.A. 101*, 8289−8294.
41. Franklin, M. C., Wang, J., and Steitz, T. A. (2001) Structure of the replicating complex of a pol α family DNA polymerase, *Cell 105*, 657−667.
42. Shamoo, Y. and Steitz, T. A. (1999) Building a replisome from interacting pieces: Sliding clamp complexed to a peptide from DNA polymerase and a polymerase editing complex, *Cell 99*, 155−166.
43. Wang, J., Sattar, A. K., Wang, C. C., Karam, J. D., Konigsberg, W. H., and Steitz, T. A. (1997) Crystal structure of a pol α family replication DNA polymerase from bacteriophage RB69, *Cell 89*, 1087−1099.
44. Comeau, S. R., Gatchell, D. W., Vajda, S., and Camacho, C. J. (2004) ClusPro: An automated docking and discrimination method for the prediction of protein complexes, *Bioinformatics 20*, 45−50.
45. Mueser, T. C., Jones, C. E., Nossal, N. G., and Hyde, C. C. (2000) Bacteriophage T4 gene 59 helicase assembly protein binds replication fork DNA. The 1.45 Å resolution crystal structure reveals a novel α-helical two-domain fold, *J. Mol. Biol. 296*, 597−612.
46. Barry, J. E. and Alberts, B. M. (1994) Purification and characterization of bacteriophage T4 gene 59 protein. a DNA helicase assembly protein involved in DNA replication, *J. Biol. Chem. 269*, 33049−33062.
47. Morrical, S. W., Beernink, H. T. H., Dash, A., and Hempstead, K. (1996) The gene 59 protein of bacteriophage T4. Characterization of protein−protein interactions with gene 32 protein, the T4 single-stranded DNA binding protein, *J. Biol. Chem. 271*, 20198−20207.
48. Xu, L. and Marians, K. J. (2003) PriA mediates DNA replication pathway choice at recombination intermediates, *Mol. Cell 11*, 817−826.
49. Liu, J. and Marians, K. J. (1999) PriA-directed assembly of a primosome on D loop DNA, *J. Biol. Chem. 274*, 25033−25041.
50. Wu, P., Nossal, N., and Benkovic, S. J. (1998) Kinetic characterization of a bacteriophage T4 antimutator DNA polymerase, *Biochemistry 37*, 14748−14755.
51. Reha-Krantz, L. J., Marquez, L. A., Elisseeva, E., Baker, R. P., Bloom, L. B., Dunford, H. B., and Goodman, M. F. (1998) The proofreading pathway of bacteriophage T4 DNA polymerase, *J. Biol. Chem. 273*, 22969−22976.
52. Baker, R. P. and Reha-Krantz, L. J. (1998) Identification of a transient excision intermediate at the crossroads between DNA polymerase extension and proofreading pathways, *Proc. Natl. Acad. Sci. U.S.A. 95*, 3507−3512.
53. Stocki, S. A., Nonay, R. L., and Reha-Krantz, L. J. (1995) Dynamics of bacteriophage T4 DNA polymerase function: Identification of amino acid residues that affect switching between polymerase and 3′ → 5′ exonuclease activities, *J. Mol. Biol. 254*, 15−28.

BI0479508